

Magnetite/ κ -carrageenan Nanocomposites: A Convenient Recyclable Tool for Cu(II) Ions Adsorption from Aqueous Solution

G. Mohammadnezhad^{a,*}, F. Ariaeinezhad^a and F. Steiniger^b

^aDepartment of Chemistry, Isfahan University of Technology, Isfahan, 84156-83111, Islamic Republic of Iran

^bCenter for Electron Microscopy, Jena University Hospital, Ziegmühlenweg 1, 07743 Jena, Germany

(Received 27 November 2019, Accepted 21 April 2020)

Exceptional 3D magnetite nanoparticles (Fe_3O_4) with high surface area, flower-like morphology, and suitable interaction with the natural polymeric matrices have been selected as inorganic nano-filler in preparation of magnetite/ κ -carrageenan nanocomposites (MCNCs). Chemical and structural properties of MCNCs were studied and characterized by ATR-FTIR, X-ray powder diffraction (XRPD), scanning and transmission electron microscopies (SEM and TEM), and thermogravimetric analyses (TGA). The MCNCs are considered as a magnetic adsorbent for adsorptive removal of contaminations such as Cu(II) from aqueous solutions. Based on adsorption data, MCNC 10 wt.% was selected for adsorption studies and different parameters including pH, contact time, and initial concentration of Cu(II) ions were optimized. The batch sorption mechanism and kinetics were estimated using three reaction kinetic models including *pseudo*-second-order, Elovich, and intra-particle diffusion. Besides, the adsorbent performance was evaluated by two common isotherm models: Langmuir and Freundlich. More significantly, kinetics and isotherm equilibrium data showed a major fitting with the intra-particle diffusion and Langmuir model, respectively. The maximum value of adsorption capacity to Cu(II) ions was found to be 22.57 mg g⁻¹ (pH = 6, adsorbent dose 0.005g (1 g l⁻¹), 25 °C, 180 rpm, and 80 min). The relative standard deviations (RSDs) for sorbent-to-sorbent reproducibility was 7.5% (n = 3). The MCNC 10 wt.% was separated easily by a supermagnet and recycled 4 times easily with the adsorption efficiency of 84% in the final cycle.

Keywords: Nanomagnetite/ κ -carrageenan nanocomposites, Adsorption, Cu(II)

INTRODUCTION

In recent years, water and environmental pollution have become one of the critical concerns of the international community. Different industries such as pigment, metallurgy, glass, and paper/textile release significant amounts of toxic heavy metal ions such as Cd(II), Cu(II), Hg(II) and Cr(VI) into the environment [1]. These are not biodegradable and have toxic, hazardous effects for both humans and environmental health, so must be eliminated from wastewater that may contact with the human body or environment [2-5].

Heavy metals toxicity can cause cardiovascular disease [6], diabetes mellitus, hypertension [7-8], cancer [6] and neurological diseases impaired intellectual ability and behavioral problems in children [9]. In this regard, advanced strategies were developed for the removal of such metal ions. A variety of methods such as ion exchange [10], solvent extraction [11], membrane filtration [12] and adsorption are used to remove significant amounts of heavy metal ions [13-18]. Among these techniques, the adsorption method is considered as one of the most common, highly efficient, and simple methods. Thus, it is considered as an economical, useful, and advantageous method in the removal of heavy metals from industrial pollutants. In this regard, different materials such as metal oxides, activated carbons, nanotubes, silicon, hydroxyapatite, and zeolites

*Corresponding author. E-mail: mohammadnezhad@iut.ac.ir

have been used as an absorbent for this process [13-17].

In recent years, polymer-based nanocomposites have attracted the attention of researchers for heavy metal removal *via* adsorption processes [19]. These mixtures have unique properties such as low cost, low toxicity [13], high chemical stability [14,19] and great adsorption performance [14], even at low concentration. In this regard, the proper selection of a polymer matrix is of great importance. Carrageenans as a member of linear negatively charged sulfated polysaccharides can be extracted from red seaweeds. They are highly flexible large molecules and could form a range of different gels at ambient temperature. There are three main commercial types of them, which are generally classified as Iota (ι), Lambda (λ), and Kappa (κ). The main differences of Iota, Kappa, and Lambda carrageenans are the position and number of the ester sulfate functionals [20-24]. Due to the presence of sulfate groups, carrageenans interact with mono and divalent ions such as calcium and can undergo conformational changes and form gels [25]. Based on their physical and chemical properties, Kappa-carrageenan forms strong, and rigid gels in the presence of K^+ ions while Iota forms soft gels in the presence of Ca^{2+} and Lambda does not form any gels [26]. Such polymers have many active sites on its surface and have individual advantages such as non-toxicity, biodegradability, low cost, and desirable chemical properties, accordingly they are found to be a suitable adsorbent for removal of heavy metal ions from industrial wastewater [13,27]. The combination of these polysaccharides with suitable inorganic nano-fillers such as Fe_3O_4 magnetic nanoparticles (MNPs) may improve their chemical and physical properties. Duman *et al.* reported magnetic carbon nanotube-Kappa-carrageenan- Fe_3O_4 nanocomposites, which have been used as adsorbents for removal of triphenylmethane, reactive azo-dyes, and cationic methylene blue [28-29]. Mahdavinia *et al.* had synthesized magnetic Kappa-carrageenan/PVA nanocomposite hydrogels for adsorption of cationic dyes [30]. Salgueiro *et al.* studied unusual dye adsorption behavior of Kappa-carrageenan coated superparamagnetic nanoparticles [31]. Daniel-da-Silva *et al.* prepared carrageenan-grafted magnetite nanoparticles and used as recyclable sorbents for dye removal [32]. Such inorganic nano-fillers, with individual properties such as 3D structure with flower-like morphology and high surface area, may

lead to better interaction with polymeric matrices [33-34].

In this paper, we prepared different novel organic-inorganic hybrid nanocomposites based on natural κ -carrageenan polymer as an organic matrix with different amounts of magnetite nanoparticles as nano-filler (5, 7 and 10 wt.%). They were characterized and used for adsorption of Cu(II) ions from aqueous solutions. The effect of different parameters such as initial Cu(II) concentration, pH, and contact time as well as their adsorption mechanism using three adsorption kinetic models and two adsorption isotherms have been studied.

EXPERIMENTAL

Materials

Cu(II) nitrate trihydrate ($Cu(NO_3)_2 \cdot 3H_2O$), iron(III) chloride hexahydrate, urea, tetrabutylammonium bromide (TBAB), hydrochloric acid and sodium hydroxide were purchased from Merck Chemical Co. Ethylene glycol (EG) was purchased from the Ameretat Shimi company and used without further purification. The κ -carrageenan powder was purchased from Refined Company. Deionized water was used in all reactions.

Instruments

FTIR spectra were recorded from 400 to 4000 cm^{-1} (Bruker, Tensor 27). Crystalline structures of the samples were examined using Siemens D5000 diffractometer (Debye Scherrer scan mode) with $Cu K_{\alpha}$ tube ($\lambda = 1.541 \text{ \AA}$) in the 2θ range of 10-90°. Thermal gravimetric analyses (TGA) were conducted under nitrogen atmosphere using NetzschStaPC409 Lexx instrument (Germany) at a heating rate of 10 $^{\circ}C \text{ min}^{-1}$ from room temperature to 800 $^{\circ}C$. The morphology of the samples was studied by SEM (Zeiss Gemini 1530, Germany) and TEM (Philips CM 120, Netherlands). A SonoSwiss ultrasonic bath (SW 3 H, Switzerland) was used at 37 kHz and power of 280 W. Cu(II) concentrations were measured by flame atomic absorption spectrophotometry (FAAS, PerkinElmer, USA).

Synthesis of Iron Glycolate Precursor and Magnetite Nanostructure

The iron glycolate precursor was prepared using ethylene glycol (EG) according to the previously published procedures [33-37]. In a typical synthesis, $FeCl_3 \cdot 6H_2O$

(1.2 g), tetrabutylammonium bromide (7.2 g), and urea (2.7 g) were added to ethylene glycol (180 ml). This mixture was stirred for 20 min at room temperature until a homogeneous red solution was obtained. Then, the solution was heated and refluxed for 2 h. The green precipitate was collected by centrifuge, washed with ethanol (three times), and dried in an oven at 80 °C for 12 h [34-36]. The green powder precursor was calcined at 450 °C under Ar atmosphere for 3 h to obtain Fe₃O₄ nanoparticles [34,36].

Synthesis of Magnetite/ κ -carrageenan Nanocomposites (MCNCs)

MCNCs with magnetite contents of 5, 7 and 10 wt.% hereafter denoted as MCNC 5 wt.%, MCNC 7 wt.%, and MCNC 10 wt.%, respectively, were prepared using a solution casting method. For the preparation of MCNCs, 0.33 g of κ -carrageenan was added to 25 ml of deionized water and the mixture was stirred with a mechanical stirrer for 1 h at 70 °C. Then, different calculated amounts of magnetite were added to 5 ml of deionized water and sonicated in an ultrasonic bath for 0.5 h. In the next step, the magnetite colloidal solution was added dropwise to the polymer matrix aqueous solution and was heated (70 °C) for 2 h, until a stable suspension was obtained. Finally, the mixtures were cast on to a Petri dish and dried at the atmospheric condition, and finally a brittle film was formed.

Adsorption Experiment

Cu(II) concentrations were measured by a flame atomic absorption spectrometer. A stock solution of Cu(II) (500 mg l⁻¹) was prepared by dissolving Cu(NO₃)₂·3H₂O in deionized water. At first, Cu(II) solutions (5 ml) with initial concentrations ranging between 10-60 mg l⁻¹ were poured into the glass containers. Then, MCNCs 0.005g (1 g l⁻¹) were added to the former solutions at room temperature, pH (2-8), and shaken for 10-120 min (180 rpm). At the end of each time intervals, the adsorbent was separated by supermagnet and washed with 1 M HCl and deionized water in order to recover the adsorbent. The adsorption capacity of MCNC 10 wt.% has been determined from the difference between the initial and the final concentrations of Cu(II) ions. Moreover, adsorption kinetic models and various equilibrium isotherm parameters were also investigated.

In utilized equipment and data analysis, the sources of

error have effectively minimized in a volumetric method such as the errors in temperature, volume, and sample mass measurements. In kinetic experiments, the sources of error including heat of reaction (thermal effects), the ratio of system volume:NCs mass, the history of the prepared samples, the experimental conditions, the magnetism of particle, and the particle size and distribution.

RESULTS AND DISCUSSION

ATR-FTIR

Figure 1 shows the ATR-FTIR spectra of Fe₃O₄ nanoparticles (a), pure κ -carrageenan (b), and MCNCs containing 5, 7, and 10 wt.% of magnetite (c, d and e). For pure Fe₃O₄ an absorption band at around 570 cm⁻¹ is related to the Fe-O vibrations frequency [38]. In the ATR-FTIR spectra of the pure κ -carrageenan as well as MCNCs, the band at 1627 cm⁻¹ is attributed to the bending vibration of water and the hydroxyl group and the band at 1225 cm⁻¹ is attributed to S-O asymmetric sulfate stretching. The absorption bands of C-O-S were observed at 845 and 850 cm⁻¹. Also, the two bands in the range of 1040-1070 cm⁻¹ are assigned to the C-O and C-OH stretching, respectively. Moreover, the MCNCs spectra confirmed the presence of the filler and showed that upon the increase of Fe₃O₄, the Fe-O absorption band at around 570 cm⁻¹ becomes more prominent [38].

X-Ray Diffraction

WAXS (wide-angle X-ray scattering) pattern of the iron glycolate precursor has been shown in Fig. 2 The pattern demonstrated a strong peak at around $2\theta = 11^\circ$, which is consistent with previous reports [34,36]. The XRD patterns of Fe₃O₄ nanoparticles and MCNCs with different Fe₃O₄ contents (5, 7 and 10 wt.%) are shown in Fig. 3. The pattern of the synthesized nano-magnetite, by thermal degradation of the alkoxide precursor, was recorded in the range of $2\theta = 10-90^\circ$. The XRD pattern of magnetite clearly exhibited eight characteristic diffraction signals, which they can be indexed as (1 1 1), (2 2 0), (3 1 1), (2 2 2), (4 0 0), (4 2 2), (5 1 1), and (4 4 0) reflections of a magnetite cubic structure and clearly confirmed the formation of highly crystalline magnetite (JCPDS = 85-1436) [24,33]. As shown in Fig. 3 the XRD pattern of MCNCs having an amorphous

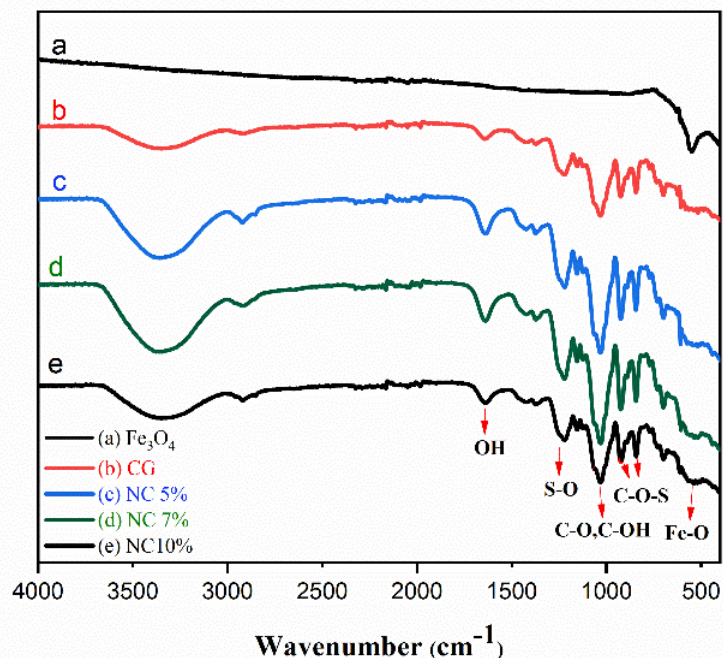


Fig. 1. ATR-FTIR spectra of (a) pure magnetite, (b) κ -carrageenan, and (c, d and e) NCs of κ -carrageenan with different amounts of flower-like magnetite.

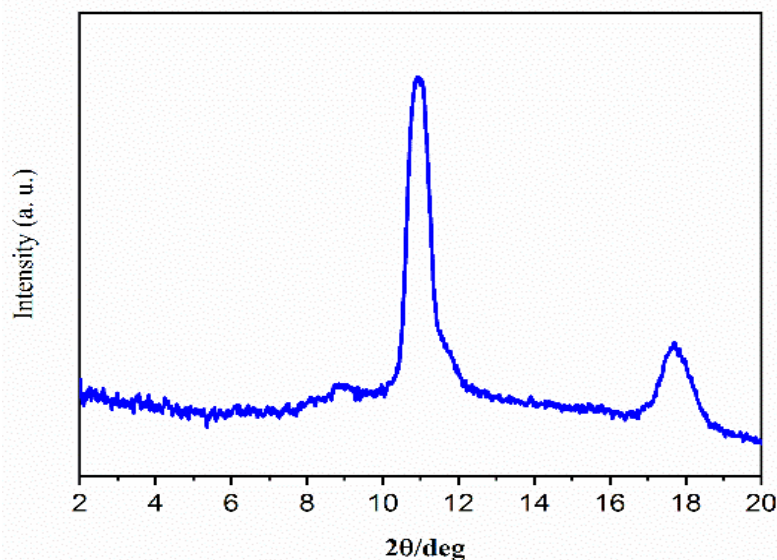


Fig. 2. WAXS pattern of the iron glycolate.

peak of κ -carrageenan at around $2\theta = 10$ - 30° as well as the patterns of Fe_3O_4 magnetite nano-filler. As we have seen in these patterns, with increasing the magnetite content, the

intensity of the magnetic's peaks has been increased while the κ -carrageenan broad amorphous peak has been decreased [20]. According to the Scherer equation modified

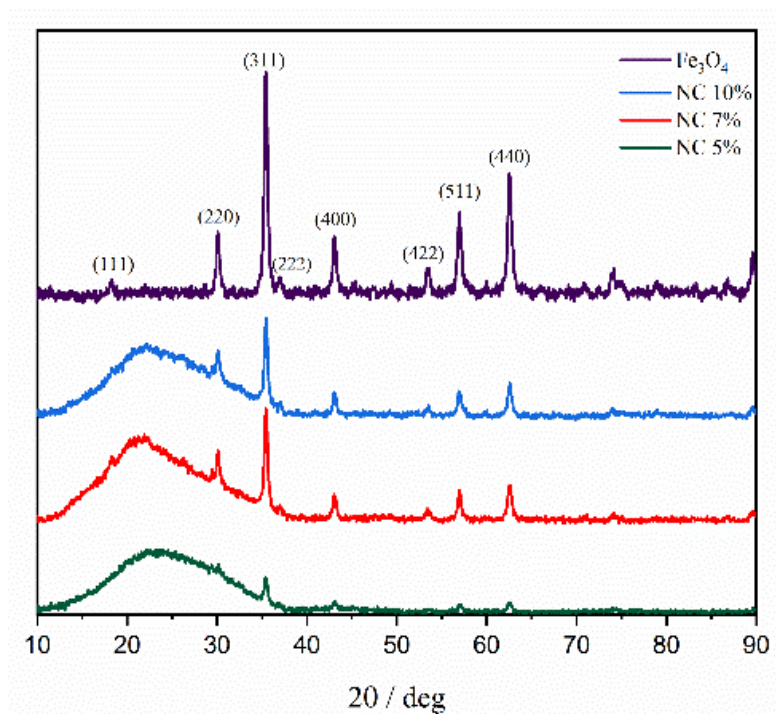


Fig. 3. XRD patterns of the magnetite and NCs of κ -carrageenan with 5, 7 and 10 wt.% of magnetite.

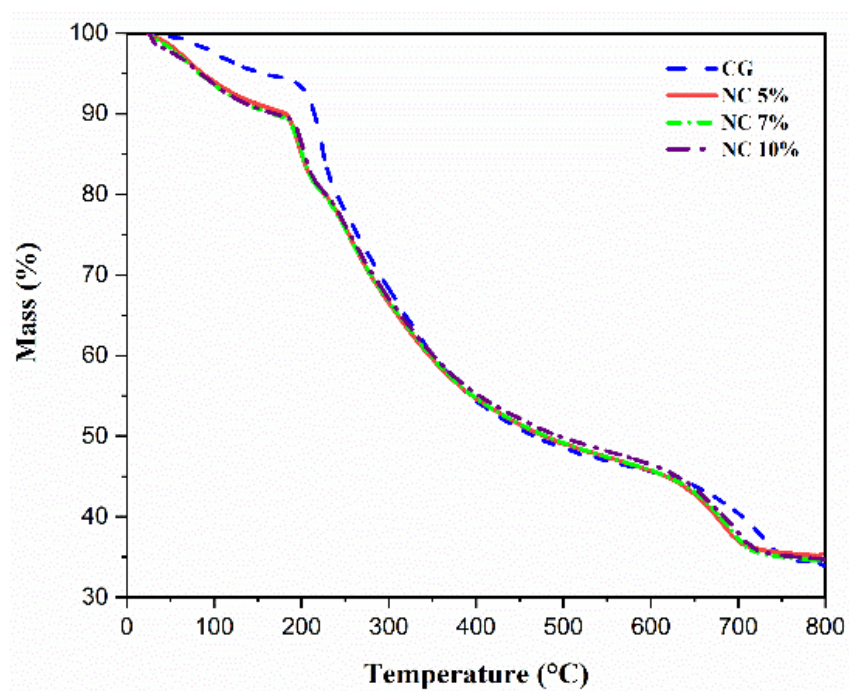


Fig. 4. TGA thermograms of the pure κ -carrageenan and NCs with 5, 7 and 10 wt.% of flower-like magnetite.

by the Williamson-Hall method, the average size of the MCNC 5 wt.%, MCNC 7 wt. % and MCNC 10 wt.% are 20.1, 22.4 and 25.2 nm, respectively (Fig. S1) [39].

Thermal Properties

The thermal behaviors of pure κ -carrageenan and the MCNCs 5, 7 and 10 wt.% were investigated by the TGA thermograms under the nitrogen atmosphere. The obtained results from the TGA analysis have shown in Fig. 4. Table 1 list different thermal parameters including T5, the temperature at which 5% loss weight happens, T10, the temperature at which 10% loss weight happens, char yield, the amount of material which is remained at 800 °C, and limiting oxygen index (LOI), the minimum oxygen concentration required for test piece to continue burning in mixed gas of oxygen and nitrogen. For the pure polymer, three weight loss steps were observed. In the first step, the removal of water and residual solvent occurs at 100-180 °C. The second step occurred from 180-600 °C, which related to the decomposition of polymer chains and organic compounds. The third step happened at 600-800 °C, which is related to the destruction of organic compounds and the formation of carbonaceous compounds. According to the obtained results, T5 and T10 of the MCNCs were lower than the pure κ -carrageenan and the degradation temperature of MCNCs was decreased with increasing the amount of nano-magnetite. According to previous studies, such results were not expected [40-41]. Usually, the introduction of inorganic nano-fillers into polymer matrix leading to an increase of thermal resistance. This odd behavior may have occurred because of the magnetic properties of the filler *i.e.* nano-magnetite might have influenced the crosslinking of the polymer chains, causing a reduction of the polymer's thermal decomposition [42-43]. Consistently, all the MCNCs showed higher char yield values compared to the pure carrageenan. LOI of a polymer can be calculated using van Krevelen and Hoftyzer equation: $LOI = 17.5 + 0.4 CY$, where CY is the char yield [44]. Self-extinguishing materials have LOI values above 21 [45]; therefore, the obtained MCNCs with LOI of *ca.* 31 can be classified as self-extinguishing materials.

Morphological Study (SEM and TEM)

Figures 5a-d showed the SEM images of the magnetite

and MCNCs 5, 7 and 10 wt.%, respectively. As shown in these figures, pure magnetite has a flower-like morphology (Fig. 5a) and each flower petal has a porous structure which resembles clinging beads formed by degradation of organic species (glycolate) of metal alkoxide by calcination with a mean size of 28 nm (inset in Fig. 5a) [34,36]. The MCNC samples showed aggregates of iron oxide particles with probable carrageenan. The carrageenan is amorphous and electron sensitive; therefore, it is easy to recognize. Moreover, TEM images showed that the magnetite nano-filler was well dispersed in the polymer matrices and created a homogeneous structure. Magnetite nano-beads are observable as semi-spherical particles in TEM images of MCNCs (Fig. 6). Based on SEM and TEM images, the average size of the MCNC 5 wt.% MCNC 7 wt.% and MCNC 10 wt.% were calculated as (20 ± 0.2) , (22 ± 0.1) , and (25 ± 0.1) nm, respectively, which is represented in the histograms (Fig. S2). The TEM results are in good agreement with the calculated results of the Scherrer equation modified Williamson-Hall method (20.1, 22.4 and 25.2 nm).

Adsorption Studies

Effect of initial concentration. In the first experiment, the adsorption of Cu(II) by MCNC 10 wt.% was studied. Accordingly, the initial concentration of Cu(II) solutions in a range between 10-60 mg l⁻¹ were varied while the adsorbent dose (0.005 g, 1 g l⁻¹), temperature (298 K), contact time (60 min) and stirring speed (180 rpm) were kept constant (Fig. 7a). As it is shown, the adsorption capacities were increased linearly upon concentrations increment from 10 to 60 mg l⁻¹. It has also been shown that the initial concentration of 10 mg l⁻¹ has the highest removal value (79%). Such trends would be as a result of the availability of the active sites in this concentration and saturation of them at higher concentrations. Therefore, 10 mg l⁻¹ was selected as an optimum concentration. Then, maximum removal values were obtained at 10 mg l⁻¹ for Fe₃O₄, kappa-carrageenan and MCNCs 5, 7, 10 wt.% as 17%, 99%, 53%, 60% and 79%, respectively (Fig. 7b). Agglomeration of the magnetite NPs in aqueous solution may hinder the accessibility of the functional groups for proper metal ions adsorption. Upon increasing magnetite moiety and better dispersion of NPs in the polymer matrix

Table 1. Thermal Properties of the Pure κ -carrageenan and MCNCs 5, 7 and 10 wt.%

Samples	Decomposition temperature			
	T_5 (°C) ^a	T_{10} (°C) ^a	Char (%) ^b	LOI ^c
κ -carrageenan	128	212	33.9	31.1
MCNC 5%	80	158	35.4	31.6
MCNC 7%	73	141	34.6	31.3
MCNC 10%	73	141	34.7	31.4

^aThe temperatures at which 5% and 10% weight losses were recorded by TGA at the heating rate of 10 °C min⁻¹ under a nitrogen atmosphere. ^bThe weight percentage of material left after TGA analysis at a temperature of 800 °C under a nitrogen atmosphere. ^cLimiting oxygen index.

as well as better dispersion of NC in aqueous solution, the adsorption values were enhanced. The increasing adsorption percentage might be related to increasing the nano-magnetite filler content since surface hydroxide and oxide groups of magnetite had suitable interactions with Cu(II) ions. Zeta potential analysis was performed for MCNC, as shown in Fig. S3. The zeta potential value for this sample was -72.6 mV that indicates the suitable surface charge of the adsorbent for the electrostatic interaction with the copper(II) cations.

Effect of pH. In order to study the influence of pH, as one of the most important factors in adsorption of Cu(II) ions, 0.005 g (1 g l⁻¹) of the adsorbent, MCNC 10 wt.%, were treated separately with 5 ml of 10 mg l⁻¹ Cu(II) ions solutions at different pHs. The pH values were adjusted by adding sodium hydroxide (0.1 M) or hydrochloric acid (0.1 M) solutions in a range of 2.0-8.0 and other parameters such as contact time (60 min), temperature (298 K) and stirring speed (180 rpm) were kept constant. Figure 8a has shown that Cu(II) adsorption has increased swiftly from pH 2.0 to 6.0 and then decreased at pH 7.0 and 8.0. The maximum adsorption value (*ca.* 88%) was obtained at pH 6, which was selected as an optimum value for adsorption experiments. At lower pH values (pH < 6), Cu(II) adsorption has been decreased due to the presence of H₃O⁺ ions and an excessive protonation of the coordinately potential functional groups of the NC including

oxygen, hydroxyl, and sulphate. In the optimized pH (*ca.* 6) the concentration of H₃O⁺ ions has been decreased and active sites with a negative charge are available to Cu(II) ions. At higher pH values (pH > 6), due to the increased hydroxyl ions concentration and interactions between Cu(II) ions with OH⁻, neutral hydroxyl precipitates or anionic complexes of hydroxide may form. So, the concentration of free forms of Cu(II) ions and their adsorption on the active sites were decreased [19].

Effect of contact time. The effect of contact time was investigated in a range of 10-120 min in 10 min time intervals at optimum pH 6, while other parameters such as temperature, adsorbent dose, initial concentration, and stirring speed were kept constant as mentioned earlier. As shown in Fig. 8b, the adsorption rate of Cu(II) ions was found to be quite fast until it reached to 80 min. The availability of active sites on the surface of the MCNC 10 wt.% and the good dispersion of adsorbent in aqueous Cu(II) solution led to 96% adsorption in 80 min. Over time, due to the saturation of adsorption locations, the adsorption amount was decreased due to the occupation of oxygen, hydroxyl, and sulfate functional groups.

Adsorption kinetics. To evaluate the adsorption effectiveness, kinetics and mechanism of the adsorption was studied. Chemical and physical properties of the adsorbents influence the adsorption mechanism. Herein, three different kinetic models, including *pseudo-second-*

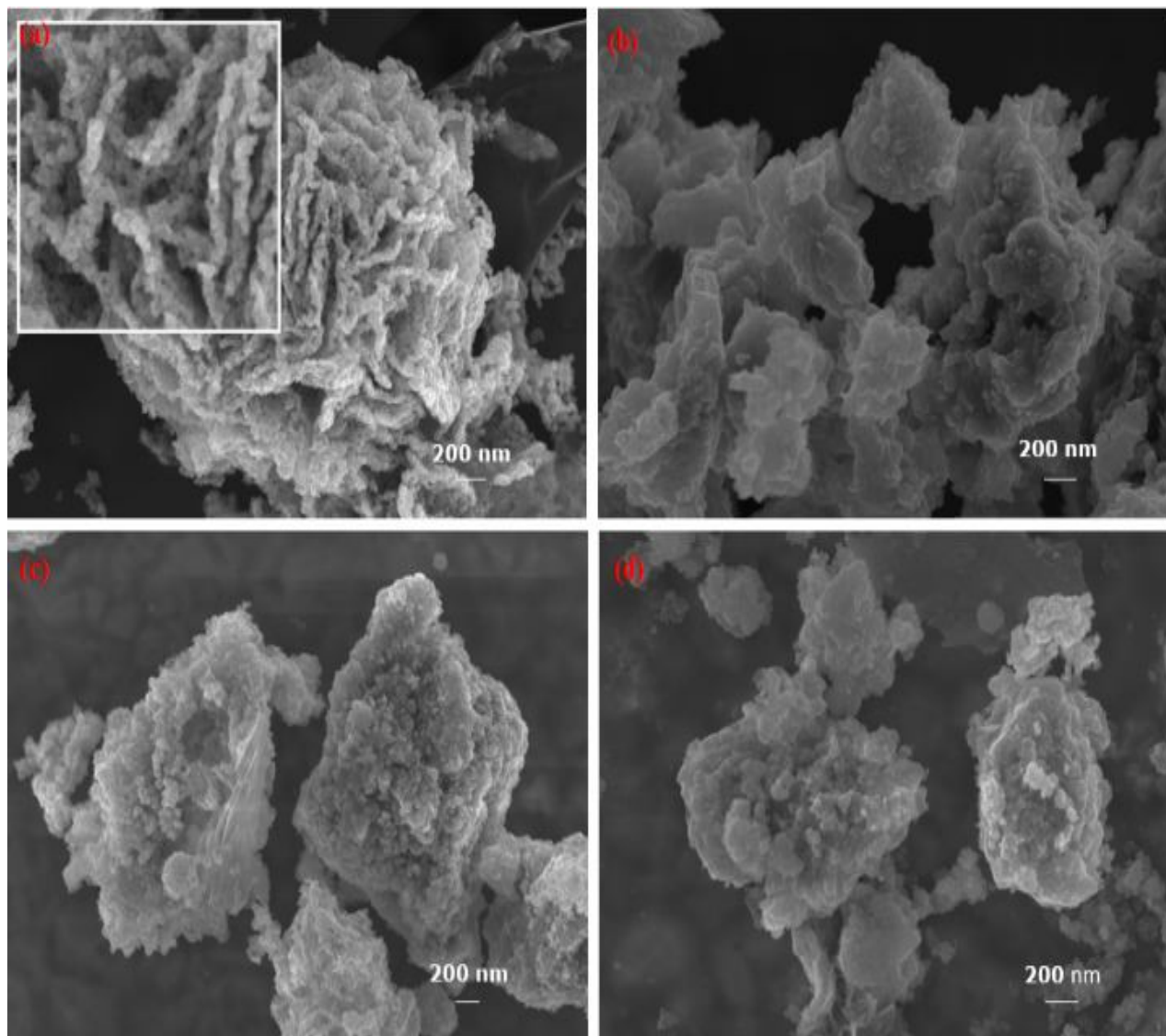


Fig. 5. SEM images of (a) magnetite (flower-like), and NCs of κ -carrageenan with (b) 5 wt.%, (c) 7 wt.% and (d) 10 wt.% of flower-like magnetite.

order, Elovich, and intra-particle diffusion, were employed.

The *pseudo*-second-order kinetic model describes that the sorption rate depends on the number of active sites on the adsorbent surface. The linear form of the *pseudo*-second-order kinetic model can be shown by Eq. (1) [45-46].

$$\frac{t}{q_t} = \frac{1}{\alpha} + \frac{1}{q_e} t \quad (1)$$

$$\alpha = k_{ad} q_e^2$$

$$q_e = \frac{(C_i - C_e)V}{m} \quad (2)$$

$$q_t = \frac{(C_i - C_t)V}{m} \quad (3)$$

The adsorption capacity, the amount of Cu(II) metal ions

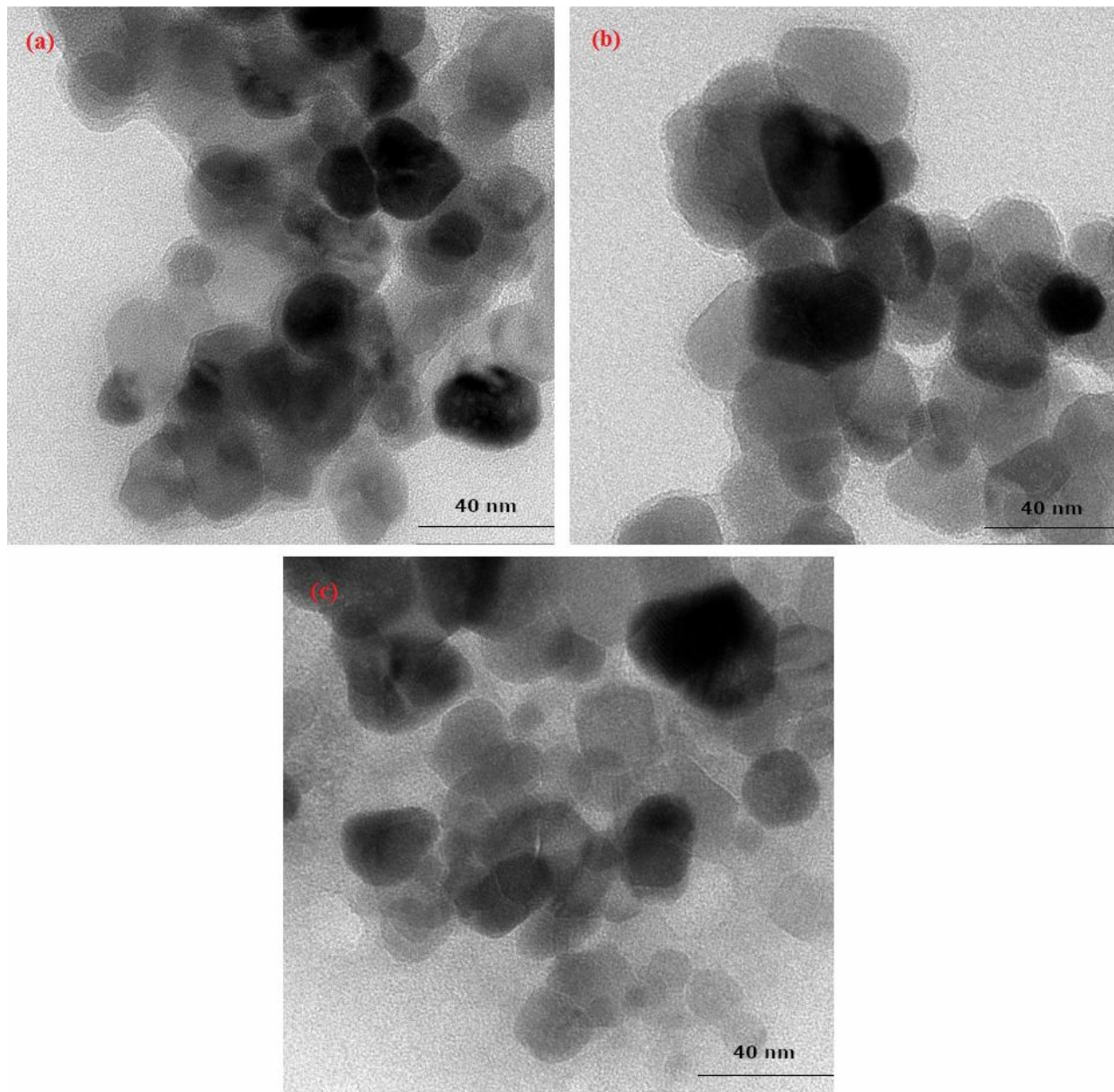


Fig. 6. TEM images of MCNCs of κ -carrageenan with (a) 5 wt.%, (b) 7 wt.% and (c) 10 wt.% of magnetite.

adsorbed, at equilibrium ($q_{e(\text{exp})}$, mg g^{-1}) and at t (q_t , mg g^{-1}) was calculated by the Eqs. (2) and (3), respectively. Also, the rate constants of *pseudo*-second-order equations (k_{ad} , $\text{g mg}^{-1} \text{min}^{-1}$) and adsorption capacity at equilibrium ($q_{e(\text{cal})}$, mg g^{-1}) can be obtained from the intercept and slope of Fig. 8b. The C_i , C_t and C_e (mg l^{-1}) are the initial, at time t , and equilibrium concentrations, respectively, V (l) is

the volume of the solution, and m (g l^{-1}) is the amount of the sorbent.

The linear form of the Elovich model can be represented by Eq. (4) [47]:

$$q_t = \frac{1}{\beta} \ln \alpha \beta + \frac{1}{\beta} \ln t \quad (4)$$

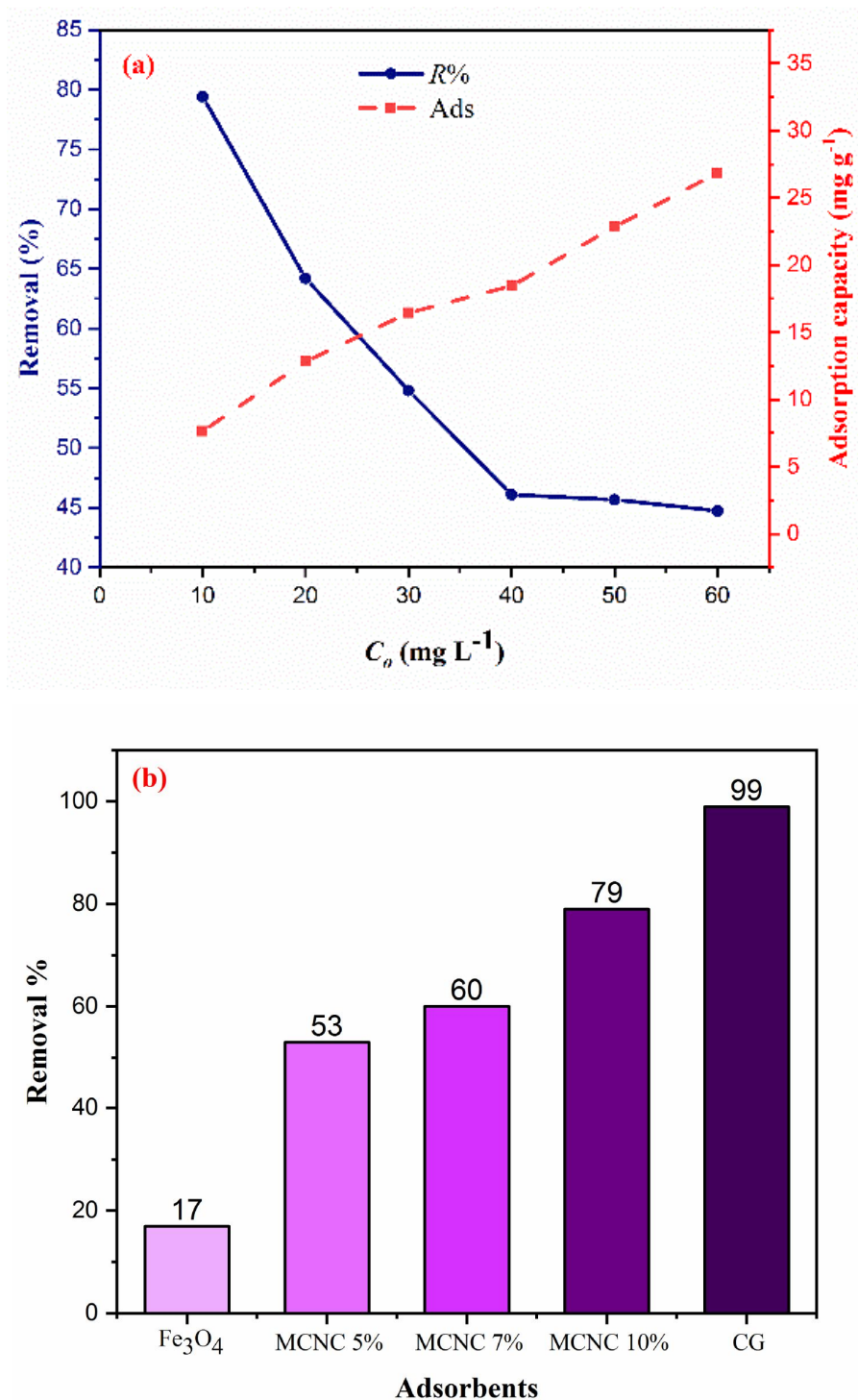


Fig. 7. The effect of initial Cu(II) concentrations on adsorption capacity and removal for MCNC 10 wt.% (a), Comparative removal efficiencies for the pure magnetite, pure κ -carrageenan, MCNCs 5, 7 and 10 wt.% (b).

Table 2. Adsorption Kinetic Parameters Fitted by *Pseudo*-second-order, Elovich and Intra-particle Diffusion Models for Removal of Cu(II) by MCNC 10 wt.%

Kinetic models	Parameters	
<i>pseudo</i> -second order	k_{ad} (g mg ⁻¹ min ⁻¹)	2.725×10^{-3}
	$q_{e (exp)}$ (mg g ⁻¹)	9.64
	q_e (mg g ⁻¹)	11.90
	R^2	0.926
Elovich	β (mg g ⁻¹ min ⁻¹)	0.283
	R^2	0.949
Intra-particle diffusion	k_{intra} (mg g ⁻¹ min ^{-1/2})	1.211
	C	-1.154
	R^2	0.966

Table 3. Adsorption Equilibrium Parameters Fitted by Langmuir, Modified Langmuir, and Freundlich Isotherm Models for Removal of Cu(II) by the MCNC 10 wt.%

Isotherm models	Parameters	
Langmuir	R^2	0.998
	K_L (l mg ⁻¹)	0.201
	q_{max} (mg g ⁻¹)	22.57
Modified Langmuir	R^2	0.998
	K_{ML} (l mg ⁻¹)	536,423
Freundlich	q_{max} (mg g ⁻¹)	22.57
	R^2	0.987
Freundlich	K_F (mg g ⁻¹)	5.38
	n	2.35

In this equation, the parameters, β and α , are defined as the adsorption constants (mg g⁻¹ min⁻¹) and initial adsorption rate (mg g⁻¹ min⁻¹), respectively. The intraparticle diffusion model refers to the transfer of species from aqueous

solutions to the solid adsorbents. Its liner form is given in Eq. (5) [48].

$$q_t = k_{intra} t^{\frac{1}{2}} + C \quad (5)$$

Where C and $k_{\text{intra}} t^{1/2}$ are rate constant and the intraparticle diffusion rate factor ($\text{mg g}^{-1} \text{min}^{-1/2}$), respectively. The kinetic parameters related to the above equations can be calculated from the slope and intercept of the linear equations, see Table 2.

According to the obtained results, it was found that the intraparticle diffusion model (Fig. 8c) provides better correlation coefficient values than the *pseudo*-second-order and Elovich models (Figs. 8b and c). Therefore, the adsorption of the Cu(II) ions could be followed by the intraparticle diffusion kinetics model. These data represented 96% adsorptive removal after 80 min. Additionally, adsorption capacities (mg g^{-1}) of different adsorbents for the removal of Cu(II) have been compared in Table 3.

Adsorption isotherm. The modified Langmuir and Freundlich adsorption isotherms are the most frequent models which were used here to examine the adsorption mechanism and interaction of Cu(II) ions with MCNC 10 wt.%. The modified Langmuir adsorption isotherm fitted with monolayer adsorption when the adsorption process occurs onto homogeneous adsorbent surfaces while the Freundlich adsorption isotherm related to multilayer adsorption process onto heterogeneous adsorbent surfaces. The linear form of the Langmuir, Freundlich, and modified Langmuir isotherm models are presented by the Eqs. (6), (7) and (8), respectively [53]:

$$\frac{C_e}{q_e} = \frac{1}{K_L q_m} + \frac{C_e}{q_m} \quad (6)$$

$$\log q_e = \log K_F + \frac{1}{n} \log C_e \quad (7)$$

$$\frac{C_e}{q_e} = \frac{C_s}{K_{ML} q_m} + \frac{(K_{ML} - 1)C_e}{K_{ML} q_m} \quad (8)$$

Where C_e (mg l^{-1}) is the equilibrium concentration of Cu(II) ions in the bulk solution, q_e is the solid phase equilibrium concentration, q_m (mg g^{-1}) is the maximum sorption capacity of adsorbent and C_s (mg l^{-1}) is the solute saturated concentration in bulk solution which is 2670 g l^{-1} for $\text{Cu}(\text{NO}_3)_2$ and K_{ML} (l mg^{-1}) is the modified Langmuir equilibrium constant. K_F and n are Freundlich isotherm

constants, which represent the adsorption capacity and adsorption intensity, respectively. The values of the saturated concentration of solutes are tabulated in solubility handbooks and other sources. The isotherm parameters related to the above equations can be calculated from the slope and intercepts of the linear forms of the equations (Fig. 8d); the results are summarized in Table 3. The Langmuir model showed a better correlation R^2 factor (> 0.99) with the experimental data than the Freundlich model, which suggests monolayer adsorption of Cu(II) onto the MCNC 10 wt.%.

Sorbent-to-Sorbent Reproducibility

The sorbent-to-sorbent reproducibility was investigated using three different MCNC 10 wt.% for adsorption of Cu(II). The relative standard deviations (RSDs) for sorbent-to-sorbent reproducibility was 7.5% ($n = 3$) that indicates the good reproducibility of the preparation procedure.

Desorption Study

Cu(II) on MCNC 10 wt.% was successfully desorbed by 10 ml of acidic solution (0.1 M HCl and deionized water) with the assistance of a mechanical shaker. Data showed that the recyclability of the MCNC 10 wt.% is efficient and practical and its performance was mainly retained while the adsorption efficiencies can reach to 84% after 4-time consecutive adsorption-desorption [54]. The result has been shown in Fig. 9.

CONCLUSIONS

In this study, novel magnetite/ κ -carrageenan nanocomposites with 5, 7 and 10 wt.% of flower-like nano magnetite were prepared simply *via* a convenient casting method. The initial experiments showed that the MCNC 10 wt.% has the best performance for adsorptive removal of Cu(II) (76%), and it was used for ongoing optimization experiments. The results showed that the highest removal efficiency achieved at the initial concentration of Cu(II) at 10 mg l^{-1} , and has been decreased at higher concentrations. Inversely, the adsorption capacities have been increased upon initial concentration increment. The optimum condition for Cu(II) adsorption was determined at an initial concentration of 10 mg l^{-1} , pH 6,

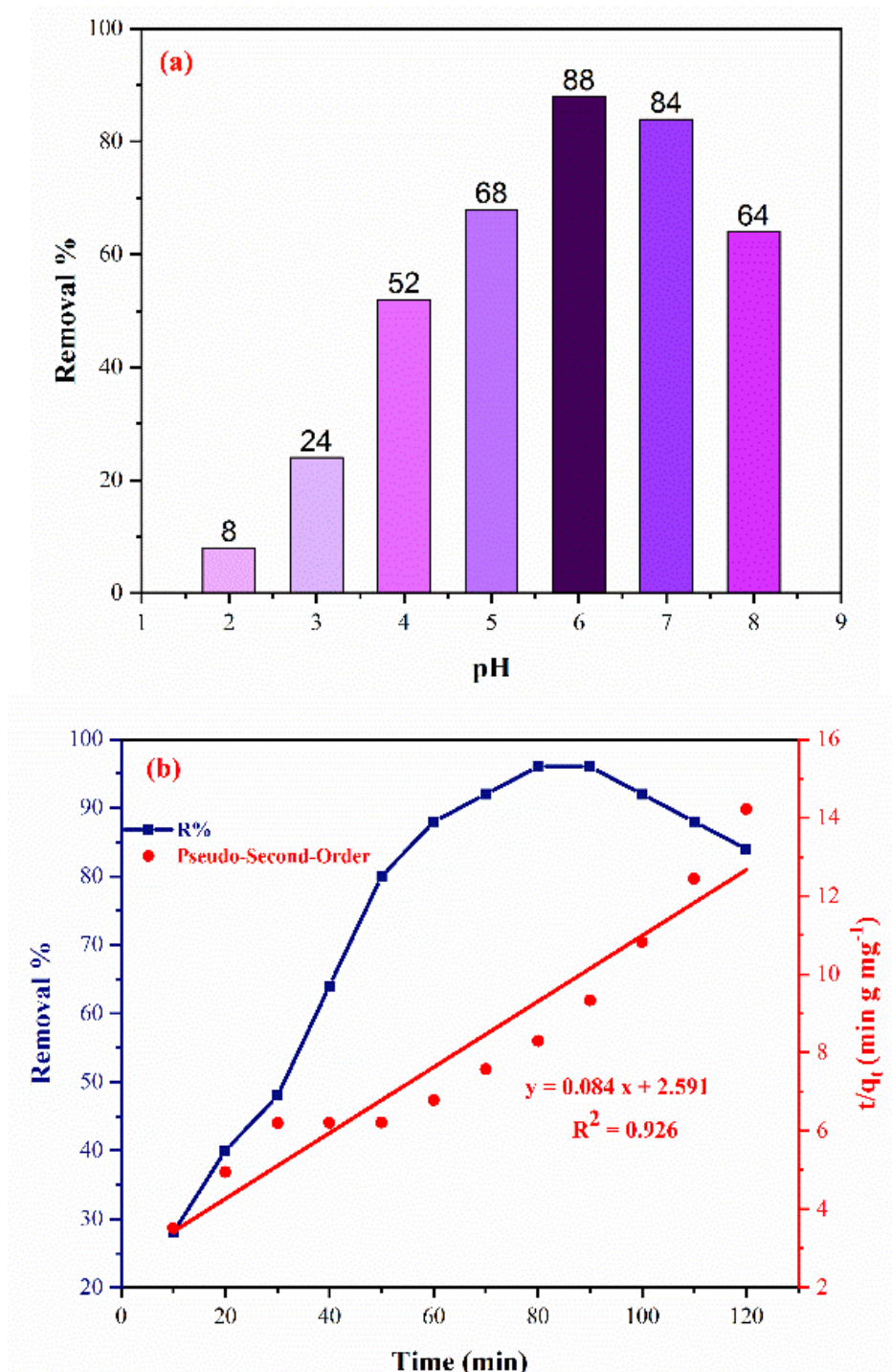


Fig. 8. Effect of pH on Cu(II) removal by the MCNC 10 wt.%, and (a) the effect of contact time on the optimum Cu(II) ions removal when the MCNC 10 wt.% was 0.005 g (1 g l⁻¹), pH = 6.0, and the Cu(II) ion concentration was 10.0 mg l⁻¹ and *Pseudo*-second-order kinetics plots of Cu(II) (b), the intra-particle diffusion and the Elovich plots (c), Langmuir and Freundlich isotherm models of Cu(II) removal by MCNC 10 wt.% (d).

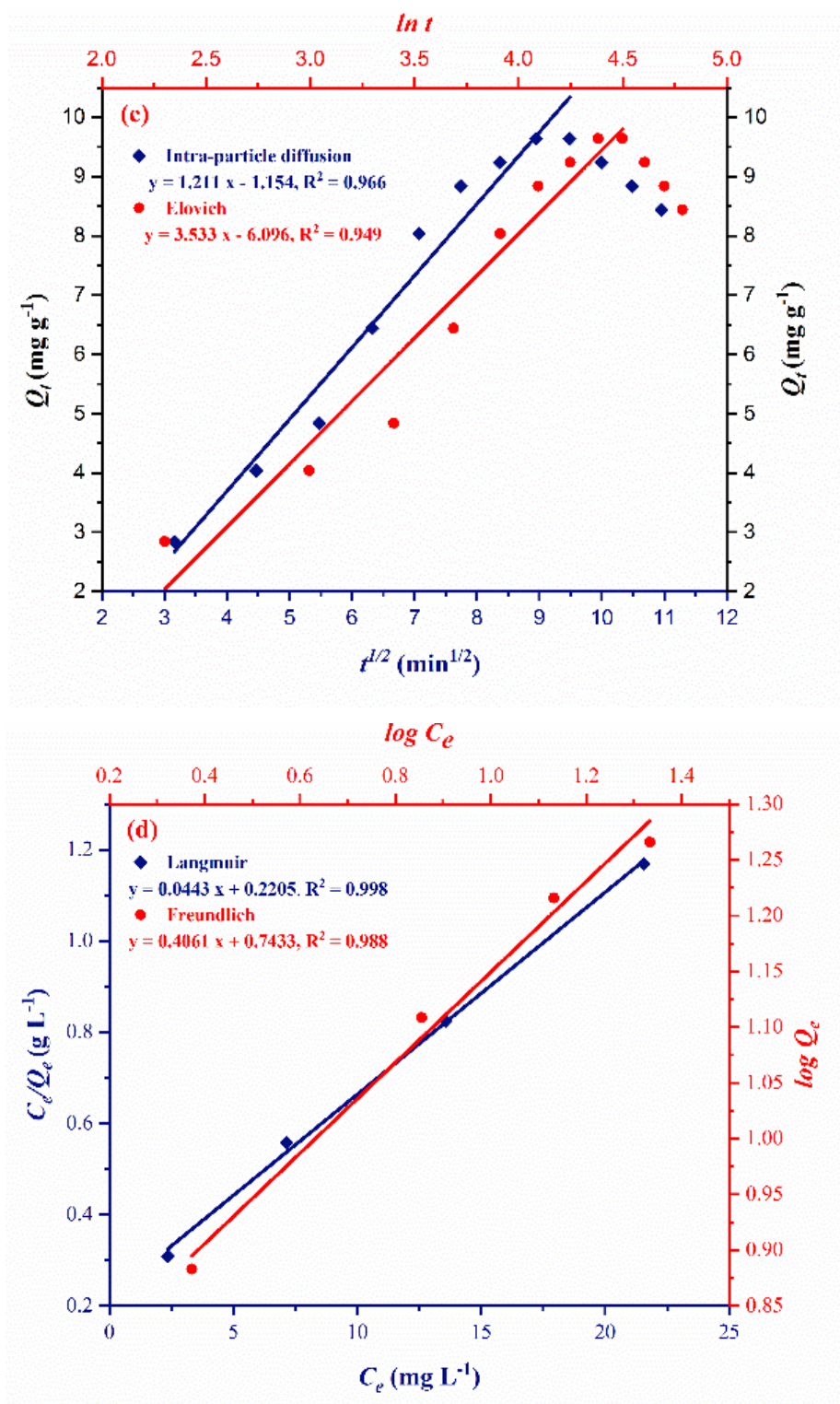


Fig. 8. Continued.

Table 4. Comparison of Adsorption Capacities toward Cu(II) Ions

Adsorbent	Adsorption capacity (mg g ⁻¹)	Isotherm models	Ref.
Platanus orientalis leaf	169.49	Langmuir	[49]
m-MCM-41/PMMA 2 wt%	40.95	Langmuir	[50]
Fe ₃ O ₄ at SiO ₂ -HA microspheres	29.42	Langmuir	[51]
Magnetite/ κ -carrageenan	22.57	Langmuir	This work
Magnetic chitosan/carrageenan composite	20.19	Langmuir	[12]
Straw/Fe ₃ O ₄ Nanocomposite	16.31	Langmuir	[52]

and equilibrium time of 80 min. The maximum adsorption capacity of Cu(II) ions by MCNCs 10 wt.% was 22.57 mg g⁻¹. The adsorption processes are described by intra-particle diffusion kinetics and modified Langmuir isotherm models. The obtained results from the two models and the experimental data were in good agreement. Cu(II) was adsorbed on MCNC 10 wt.% successfully and desorbed by using HCl solution. 4-time consecutive adsorption-desorption of Cu(II) on MCNC 10 wt.% validates the feasibility of Cu(II) desorption.

ACKNOWLEDGMENTS

Partial financial support from the Research Affairs Division of Isfahan University of Technology (IUT) is acknowledged.

Conflict of Interest

On behalf of all authors, the corresponding author states that there is no conflict of interest.

REFERENCES

- [1] Y. Chen, L. Chen, H. Bai, L. Li, *J. Mater. Chem. A* 6 (2013) 1992.
- [2] G. Mohammadnezhad, A. Keikavousi Behbahan, *J. Iran Chem. Soc.* (2020). <https://doi.org/10.1007/s13738-020-01864-8>.
- [3] Y. Luo, W. Guo, H.H. Ngo, L.D. Nghiem, F. Hai, J. Zhang, Sh. Liang, X.C. Wang, *Sci. Total Environ.* 473 (2014) 619.
- [4] W. Baran, E. Adamek, J. Ziemiańska, A. Sobczak, *J. Hazard. Mater.* 196 (2011) 1.
- [5] M. Chahkandi, A. Amiri, *Inorg. Chem. Res.* 2 (2019) 50.
- [6] E.M. Alissa, G.A. Ferns, *J. Toxicol.* 2011 (2011).
- [7] A. Navas-Acien, E.K. Silbergeld, A.R. Sharrett, E. Calderon-Aranda, E. Selvin, E. Guallar, *Environ. Health Perspect.* 113 (2005) 164.
- [8] W.C. Prozialeck, J.R. Edwards, J.M. Woods, *Life Sci.* 79 (2006) 1493.
- [9] R.A. Goyer, *Environ. Health Perspect.* 100 (1993) 177.
- [10] H. Simsek, M. Kobya, E. Khan, A.N. Bezbaruah, *Environ. Technol.* 36 (2015) 1612.
- [11] Y. Zhou, S. Boudesocque, A. Mohamadou, L. Dupont, *Sep. Sci. Technol.* 50 (2015) 38.
- [12] M. Monti, G. Camino, *Polym. Degrad. Stab.* 98 (2013) 1838.
- [13] X. Liang, J. Duan, Q. Xu, X. Wei, A. Lu, L. Zhang, *Chem. Eng. J.* 317 (2017) 766.
- [14] O.F. Gonzalez Vazquez, M.D.R. Moreno Virgen, V. Hernandez Montoya, R. Tovar Gomez, J.L. Alcantara Flores, M.A. Perez Cruz, M.A. Montes Moran, *Ind. Eng. Chem. Res.* 55 (2016) 9323.
- [15] N. Gupta, A.K. Kushwaha, M.C. Chattopadhyaya,

- Adv. Mater. Lett. 2 (2011) 309.
- [16] M.S. Ivanovic, I. Smiciklas, S. Pejanovic, Chem. Eng. J. 223 (2013) 833.
- [17] Y. Zhan, J. Lin, J. Li, Environ. Sci. Pollut. R. 20 (2013) 2512.
- [18] M.R. Awual, G.E. Eldesoky, T. Yaita, M. Naushad, H. Shiwaku, Z.A. AlOthman, Sh. Suzuki, Chem. Eng. J. 279 (2015) 639.
- [19] G. Mohammadnezhad, S. Abad, R. Soltani, M. Dinari, Ultrason. Sonochem. 39 (2017) 765.
- [20] S. Rostamnia, B. Zeynizadeh, E. Doustkhah, A. Baghban, K. Ojaghi Aghabash, Catal. Commun. 68 (2015) 77.
- [21] F. Jones, H. Colfen, M. Antonietti, Biomacromolecules 1 (2000) 556.
- [22] A.L.D. Da Silva, A.M. Salgueiro, S. Fateixa, J. Moreira, A.C. Estrada, A.M. Gil, T. Trindade, Mater. Res. Soc. Symp. Proc. 1403 (2012).
- [23] S. Roy, J.W. Rhim, Food Hydrocoll. 90 (2019) 500.
- [24] J. Long, X. Yu, E. Xu, Zh. Wu, X. Xu, Zh. Jin, A. Jiao, Carbohydr. Polym. 131 (2015) 98.
- [25] P. Versluis, A.K. Popp, K.P. Velikov, Langmuir. 27 (2011) 83.
- [26] M.Y. Kariduraganavar, A.A. Kittur, R.R. Kamble, Natural and Synthetic Biomedical Polymers, Elsevier. (2014) 1.
- [27] T.K. Giri, D. Verma, D.K. Tripathi, Polym. Bull. 72 (2015) 1625.
- [28] O. Duman, S. Tunç, B.K. Bozoğlan, T.G. Polat, J. Alloys Compd. 687 (2016) 370.
- [29] O. Duman, S. Tunç, T.G. Polat, B.K. Bozoğlan, Carbohydr. Polym. 147 (2016) 79.
- [30] G.R. Mahdavinia, A. Massoudi, A. Baghban, E. Shokri, J. Environ. Chem. Eng. 2 (2014) 1578.
- [31] A.M. Salgueiro, A.L. Daniel-da-Silva, A.V. Girão, P.C. Pinheiro, T. Trindade, Chem. Eng. J. 229 (2013) 276.
- [32] A.L. Daniel-da-Silva, A.M. Salgueiro, B. Creaney, R. Oliveira-Silva, N.J. Silva, T. Trindade, J. Nanoparticle Res. 17 (2015) 302.
- [33] L.S. Zhong, J.S. Hu, H.P. Liang, A.M. Cao, W.G. Song, L.J. Wan, Adv. Mater. 18 (2006) 2426.
- [34] X. Li, B. Zhang, Ch. Ju, X. Han, Y. Du, P. Xu, J. Phys. Chem. C. 115 (2011) 12350.
- [35] S. Shivakumara, T.R. Penki, N. Munichandraiah, ECS Electrochem. Lett. 2 (2013) A60.
- [36] D. Wang, P. Yang, B. Huang, Mater. Res. Bull. 73 (2016) 56.
- [37] J.J. Zhang, Y.L. Chen, Y.F. Sun, T. Huang, A.S. Yu, RSC Adv. 3 (2013) 20639.
- [38] A.L. Daniel-da-Silva, R. Loio, J.A. Lopes-da-Silva, T. Trindade, B.J. Goodfellow, A.M. Gil, J. Colloid Interface Sci. 324 (2008) 205.
- [39] G. Singla, K. Singh, O.P. Pandey, Appl. Phys. A. 113 (2013) 237.
- [40] A. Laachachi, M. Ferriolb, M. Cochezb, J.M. Lopez Cuestac, D. Ruch, Polym. Degrad. Stabil. 94 (2009) 1373.
- [41] Y.S. Lipatov, V.F. Rosovitskii, V.F. Babich, J. Appl. Polym. Sci. 20 (1976) 1787.
- [42] D.J. Maciel, I.L. De Mello Ferreira, G.M. Da Costa, M.R. Da Silva, Eur. Polym. J. 76 (2016) 147.
- [43] P. Wang, M. Du, Zh. Han, Sh. Bao, T. Yang, M. Zou, J. Hazard. Mater. 286 (2015) 533.
- [44] D.W. Van Krevelen, P.J. Hoflyzer (3rd ed), Properties of Polymers, Elsevier Scientific Publishing, New York, 1976.
- [45] S. Azizian, J. Colloid Interface Sci. 276 (2004) 47-52.
- [46] Y.S. Ho, D.A.J. Wase, C.F. Forster, Environ. Technol. 17 (1996) 71.
- [47] Y. Sh. Ho, J Hazard. Mater. 136 (2006) 681.
- [48] C. Namasivayam, K. Ranganathan, Water Res. 29 (1995) 1737.
- [49] S. Abadian, A. Rahbar-Kelishami, R. Norouzbeigi, M. Peydayesh, Res. Chem. Intermed. 41 (2015) 7669.
- [50] G. Mohammadnezhad, P. Moshiri, M. Dinari, F. Steiniger, J. Iran. Chem. Soc. 16 (2019) 1491.
- [51] Sh. Lan, X. Wu, L. Li, M. Li, F. Guo, Sh. Gan, Colloids Surf. A. 425 (2013) 42.
- [52] R. Khandanlou, M.B. Ahmad, H.R.F. Masoumi, K. Shameli, M. Basri, K. Kalantari, PloS one 10 (2015) e0120264.
- [53] S. Azizian, S. Eris, L.D. Wilson, Chem. Phys. 513 (2018) 99.
- [54] X. Liu, Q. Hu, Z. Fang, X. Zhang, B. Zhang, Langmuir. 25 (2008) 3.